Philosophical Magazine
Vol. 91, No. 12, 21 April 2011, 1693–1704

Taylor & Francis
Taylor & Francis Group

Time-dependent Benioff strain release diagrams

V. Frid[a], J. Goldbaum[b]*, A. Rabinovitch[c] and D. Bahat[d]

[a]*Geotechnical Department, Isotop Ltd., Canot Industry Zone, Israel;* [b]*Physics Department, Technological College, Beer Sheva, Israel;* [c]*Physics Department, Ben Gurion University, Beer Sheva, Israel;* [d]*Geological and Environmental Sciences Department, Ben Gurion University, Beer Sheva, Israel*

(*Received 25 February 2010; final version received 27 November 2010*)

New time-dependent Benioff strain (TDBS) release diagrams were analyzed for acoustic emission during various loading tests and for electromagnetic (EM) radiation emanating during compression and, tension, which end in failure. TDBS diagrams are Benioff diagrams that are built consecutively, each time using a greater number of events (acoustic or EM emissions) using the last event as if it were associated with the 'actual failure'. An examination of such TDBS diagrams shows that at a certain time point (this time point is denoted by the term 'alarm' time), a comparatively short interval prior to actual collapse, their decreasing part is broken by a positive 'bulge'. This 'bulge' is quantified and an algorithm proposed for its assessment. Using the alarm time and other parameters of the failure process (fall, bulge size and escalation factors, bulge slope and slope fall time), a criterion for estimating the time of the actual collapse is developed and shown to agree well with laboratory experimental results.

Keywords: Benioff strain; acoustic emission; electromagnetic radiation; failure process

1. Introduction

The objective of this article is to report time-dependent Benioff strain (TDBS) release rate diagrams and to define features that would yield a possibility of forecasting an oncoming failure. Benioff strain release diagrams (see, for example, Kossobokov et al. [1]) are specific bilogarithmic curves relating strain release, i.e. the square root of the energy, with 'current time' (usually in reverse order). They are often used to characterize failure (e.g. earthquakes [2,3]) associated with a so-called 'accelerated fracture release', but only after its appearance.

1.1. *Accelerated fracture release*

The phenomenon of accelerated fracture release (AFR) is found prior to about 10–30% of all earthquakes [4] and is considered by scientists to be their possible precursor (see, for example, [5]). It is now known that the AFR is a critical

*Corresponding author. Email: julia@bgu.ac.il

ISSN 1478–6435 print/ISSN 1478–6443 online

DOI: 10.1080/14786435.2010.544684
http://www.informaworld.com

phenomenon, which culminates in a 'large' event – the critical point [6]. Bufe and Varnes [7] applied the following power-law time-to-failure relationship to the changes in AFR preceding large earthquakes (EQs) in the San Francisco Bay area

$$d\Omega/dt = k(t_c - t)^m, \tag{1}$$

where Ω is some measurable quantity describing the rate of fracturing (event count, or Benioff strain), t_c is the time of the large EQ, t is the time of measurement of $d\Omega/dt$, and k and m are constants. They showed that Equation (1) leads to accurate enough predictions of the time of the oncoming macro-fracturing.

However, it is almost impossible to find the three parameters k, m and t_c (in order to use Equation (1) to forecast failure time) by a least squares method. The reason is that the three are interdependent, and a local minimum is often encountered. Thus, not only the failure time t_c cannot be predicted properly by applying a least-squares fit to Equation (1), but also its error cannot be estimated. That is, 'predictions' using Equation (1) can be made only when the failure event has happened, because otherwise t_c is not known.

Zhang et al. [8] studied acoustic emission during rock fracture in tri-axial tests. They noted that it was possible to obtain an alarm some time before failure takes place.

In this paper, a specific procedure is developed that enables us to obtain an alarm, which makes it possible to estimate the oncoming failure time without knowing the stress history.

1.2. *Benioff strain release and diagrams*

Benioff strain release is the square root of the energy released in some sub-failure process prior to actual collapse. Since the energy of electromagnetic radiation (EMR) or acoustic emission is known to be proportional to the square of the pulse maximal amplitude, the Benioff strain release of EMR or acoustic emission is simply a measure of the pulse amplitude.

Cumulative Benioff strain release, given by $S = \sum E_i^{1/2}$, is believed to be a helpful clue for forecasting the failure event. It was noted by Kawada and Nagahama [9] that the cumulative Benioff strain release was due to time-scale invariant evolution of damage. Kawada et al. [10] studied cumulative Benioff electromagnetic radiation in laboratory failure tests, along with cumulative Benioff strain release before an upcoming earthquake, and showed the similarity in their features. Zhang et al. [8] developed a useful procedure that can give information about the oncoming failure.

In Benioff diagrams data is presented in a bilogarithmic scale, where the x-axis measures backward 'relative time' given by

$$\bar{t} = 1 - \frac{t - t_i}{t_c - t_i} = \frac{t_c - t}{t_c - t_i}, \tag{2}$$

where t is the current time, t_i is the time of the whole process initiation, that is, the first event time, and t_c is the collapse time. Thus, the relative time of collapse is 0 while the relative time equals 1 when the first event was registered. The y-axis shows the cumulative Benioff strain release, S.

This presentation method enables one to divide the failure process into three principal stages: nucleation, intermediate and irreversible (see [11] and Figure 2). It is the latter stage that is of interest in our procedure. In order to obtain information on the oncoming failure time, several Benioff diagrams are built, each one using information that is available at that moment. The method is described in Section 2.

1.3. *A brief description of the electromagnetic radiation (EMR) from fractures*

The EMR phenomenon has been measured in fracturing in different materials, including metals, alloys, single crystals, rock and ice [12–18].

Our analysis ([13] and references therein) showed that that the EMR mechanism is invariant according to: (i) the type of material fractured (brittle and amorphous, rock and man-made), (ii) the fracturing scale. Rabinovitch et al. [11], analyzing EMR amplitude changes induced by rock compression, showed a similarity in the fractal nature of the processes controlling earthquakes and starquakes and those in operation for EMR induced by rock fracture, and noted that a basic general process could be 'acting behind' all these phenomena. A similar result was recently observed [14] in pressure-stimulated current.

2. Method and data

2.1. *Data and method of presentation*

2.1.1. *EMR experiments*

During our uniaxial and tri-axial compression experiments the measurement assemblage was as follows [13]. A tri-axial load frame (TerraTek stiff press model FX-S-33090; axial pressure up to 450 MPa; confining pressure up to 70 MPa; stiffness 5×10^9 N/m) was used for the measurement. It is combined with a closed-loop servocontrol (linearity 0.05%), which was used to maintain a constant axial piston rate of displacement. The load was measured with a sensitive load cell (LC-222 M, maximum capacity 220 kN, linearity 0.5% full scale). The confining pressure was continually controlled by a clock-type sensor to preserve its preset value through volumetric changes of the sample during the loading process. The cantilever set (consisting of axial and lateral detectors; strain range about 10%; linearity 1% full scale) enabled us to measure sample strains in three orthogonal directions, parallel to the three principal stresses. A magnetic one-loop antenna (EHFP-30 Near Field Probe set, Electro-Metrics Penril Corporation) 3 cm in diameter was used for the detection of the EMR. It is wound within a balanced Faraday shield, so that its response to external electric fields is vanishingly small. A low-noise microsignal amplifier (Mitek Corporation Ltd., frequency range 10 kHz–500 MHz, gain 60 ± 0.5 dB, noise level 1.4 ± 0.1 dB across the entire frequency band) and a Tecktronix TDS 420 digital storage oscilloscope connected by means of a General Purpose Interface bus to an IBM PC, completed the detection equipment. The entire system 'antenna–amplifier–storage oscilloscope', was carefully adjusted to an input–output impedance of 50 Ω. The antenna was placed 2 cm away from the center of the loaded samples with its normal pointing perpendicular to the cylinder axis.

The EMR was monitored in the frequency band from 10 kHz up to 50 MHz with an overall sensitivity of up to 1 μV.

The measurement assemblage for our tension [19] experiments was very similar to the one given above. A TerraTek tension machine (maximal axial stress up to 100 MPa; stiffness 5×10^9 N/m) was used for the measurement during the tension experiments. It is operated by a closed-loop servocontrol (linearity 0.05%), which is used to maintain a constant axial piston rate of displacement. The axial load was measured with a load cell (linearity 0.5% full scale). Each sample was uniaxially loaded by an axial displacement rate of 1 μm/s. The same magnetic one-loop antenna (situated 2 cm away from the center of the loaded samples with its normal pointing perpendicular to the cylinder axis) and electronic system as in two above experimental setups were employed for the study.

All the samples with the antenna were placed in a Faraday cage. All EMR signals were electrically amplified by 60 dB, digitized and collected by a PC hard disk. The data was analyzed after the tests were completed.

2.1.2. *Analysis*

We analyzed data for EMR [19] observations (see Subsection 2.1.1 for experimental details) during (i) one-dimensional (1D) and three-dimensional (3D) lab compression of chalk samples (23 samples, 462 events), and (ii) direct failure in tension of soda lime glass and Solenhoffen limestone (4 samples, 530 events) [19]. Acoustic emission (AE) data obtained during loading of several materials [20] under compressional loading (with constant pressure, 104 events; with erratic pressure, 68 events) and tensional loading (31 events) were also analyzed. In our EMR experiments, we used several samples for each loading type. Instead of presenting these samples separately, we present them in the same graph. Figure 1 shows examples of EMR observations during 3D compression of chalk samples, and in direct tension [19], whereas Figure 2 shows the same data in the form of Benioff strain release diagrams. Figure 3 shows AE events induced by compression and tension in the experiments of Guarino et al. [20] in the form of Benioff strain release diagrams.

Note that in Figure 2, during the nucleation stage, the graphs are almost vertical; during the intermediate stage their log–log slope changes rapidly and is 'decorated' by periodic variations, whereas in the irreversible stage the slope decreases monotonically and slowly. This behavior implies that the irreversible stage is preceded by a relatively rapid turning of slope. This slope change prior to the irreversible stage of the Benioff strain release diagram could be a possible indicator of an oncoming sample failure. This indication however seems to be only hindsight since the diagram is constructed only when failure time is already known. To overcome this limitation we propose a method of building a new time dependent diagram for which no prior knowledge of t_c is necessary.

Assume t_0 is the time of measurement beginning. Starting at time t_0 we collect a certain amount of events, say 10, before continuing. Now, if the next event (after previous 10) occurred at time t_1 we suppose this time as a virtual (fake)

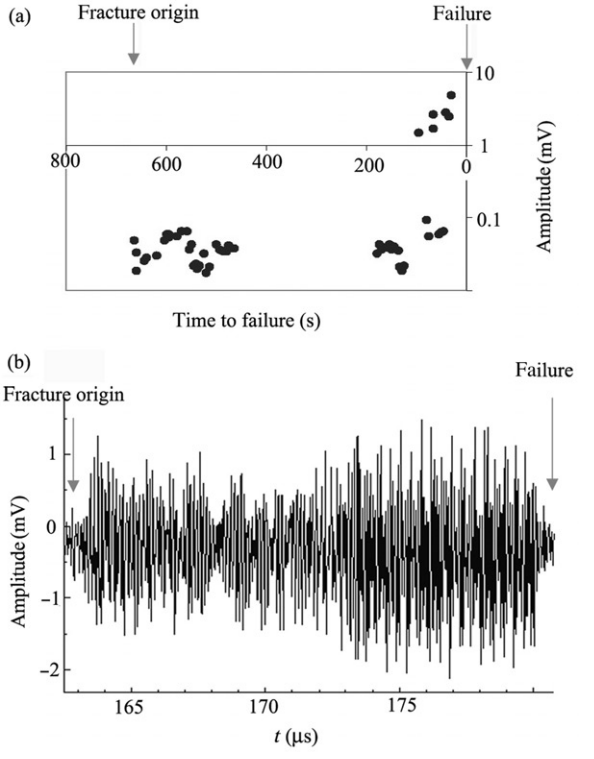

Figure 1. (a) An example of EMR observation during 3D compression of a chalk sample. The *x*-axis shows time to final failure, while the *y*-axis is the amplitude of EMR signals in mV shown in the logarithmic scale. (b) EMR event induced by direct tension of soda lime glass. The lengthy signal registered is also consisting of a chain of high frequency EMR pulses [19]: the first EMR pulse in this chain was the first registered during the drilling and the last EMR pulse in the chain was the last one registered by us during the experiment.

collapse time: t_{vc} ($=t_1$), and define a virtual relative time to failure $\bar{t}_v$ according to Equation (2):

$$\bar{t}_v = \frac{t_{vc} - t}{t_{vc} - t_0}. \tag{3}$$

We now use the last few points in the cumulative virtual (time dependent) Benioff diagram (i.e. log(total energy)$^{1/2}$as a function of $(-\log \bar{t}_v)$, where the total energy is summed up from t_0 on) to calculate the 'virtual irreversible slope' (VIS).

As events further accumulate, t_1 would change along with t_{vc}, $\bar{t}_v$, the cumulative virtual Benioff release and the VIS, yielding a function of VIS vs. t_1 whose number of points increases by one with every new recorded set of events.

Figure 4 shows two examples of such slopes for our compression and tension tests. As is seen, both graphs have some common qualitative features: a falloff of the slope at the beginning of the process (the first two to three intervals) with a further 'slow' slope decrease, broken by at least one bulge before failure.

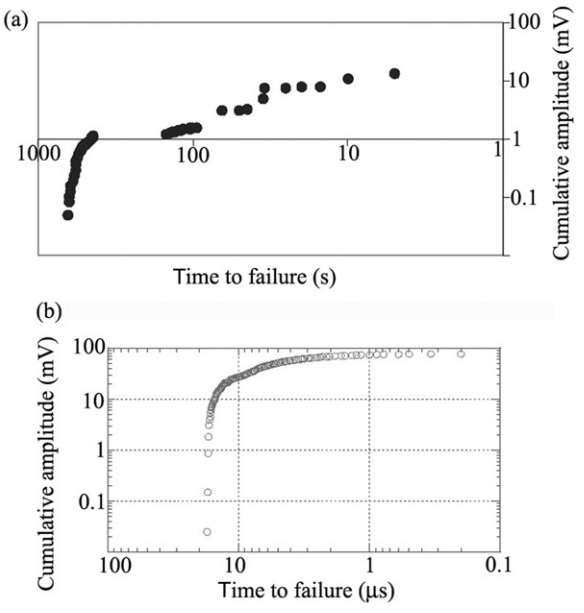

Figure 2. Benioff strain release graphs of the amplitude of EMR induced by chalk 3D compression (a) and tension (b).

To qualitatively characterize these graphs, consider their key points (Figure 5). We denote the initial slope (at t_1) by m_i, the slope at the last point prior to the 'bulge' by m_f, the slope at the 'bulge' itself by m_a and the time from process origin up to the bulge by t_a. (Note that when no failure is expected, the emission (Benioff strain) rate does not increase with time, and no bulge appears in the graph.)

The following parameters are employed in the analysis: the fall factor, $M_{if} = m_i/m_f$; the bulge size factor, $M_1 = (m_a - m_f)/m_f$; and the escalation factor of the Benioff strain release: $L_s = \log(\Sigma S_f/S_1)$, where ΣS_f is the cumulative Benioff strain release up to the time corresponding to m_f, and S_1 is Benioff strain release at the first registered event. Note that no parameter considered includes t_c.

3. Results and discussion

3.1. *'Slope at bulge' definition and criterion*

As mentioned, we consider here five different processes. The averaged essential data for the processes are given in Table 1. The data pertain to different types of loading (see above) and two types of emissions. Hence, though not many, our data encompasses a whole range of phenomena. Note that we just put forward a new method of Benioff strain-release analysis and that more accurate values of the considered parameters could definitely be found by future detailed statistical analysis. Our analysis showed however that for all considered cases the value of the slope at the 'bulge', m_a, the escalation factor, L_s, and the

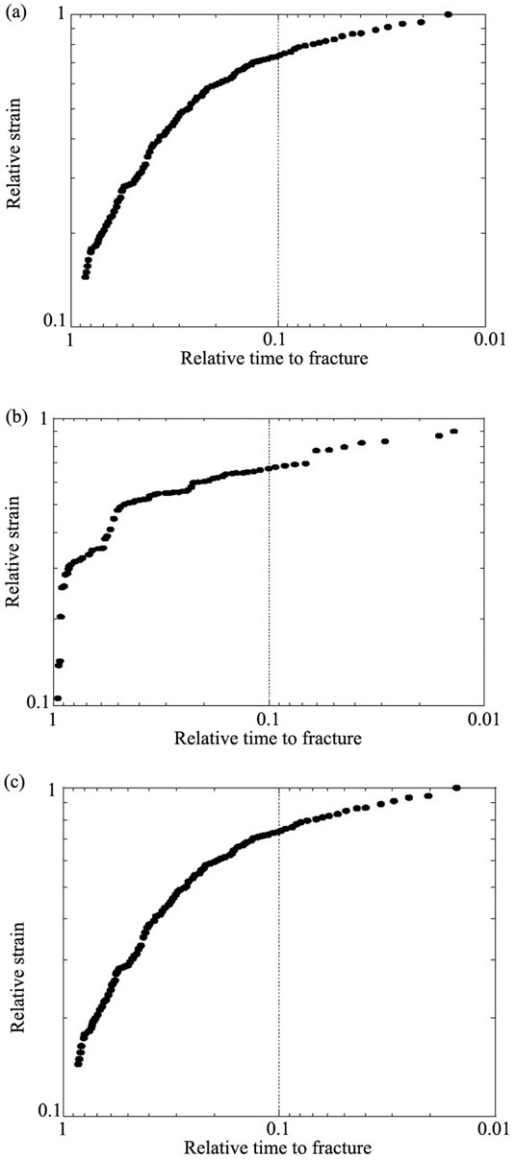

Figure 3. Cumulative Benioff release of acoustic emission (in relative units, normalized to be 1 at failure) emanated during sample failure under (a) constant load, (b) erratic load, (c) tension load [20].

number of events, N, registered up to the 'bulge moment' fit the following empirical relationship:

$$m_a(1 + L_s) = \frac{0.016}{N^{\alpha}}, \tag{4}$$

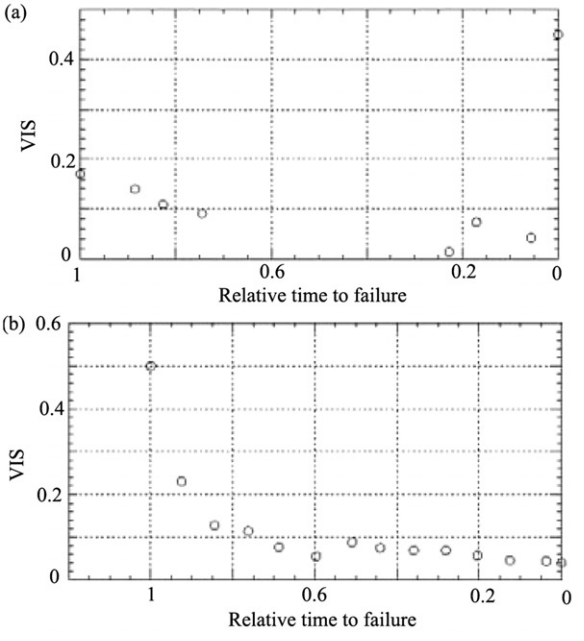

Figure 4. Three examples of graphs of the slope of the bilogarithmic TDBS curves as a function of relative time to failure: (a) compression; (b) tension.

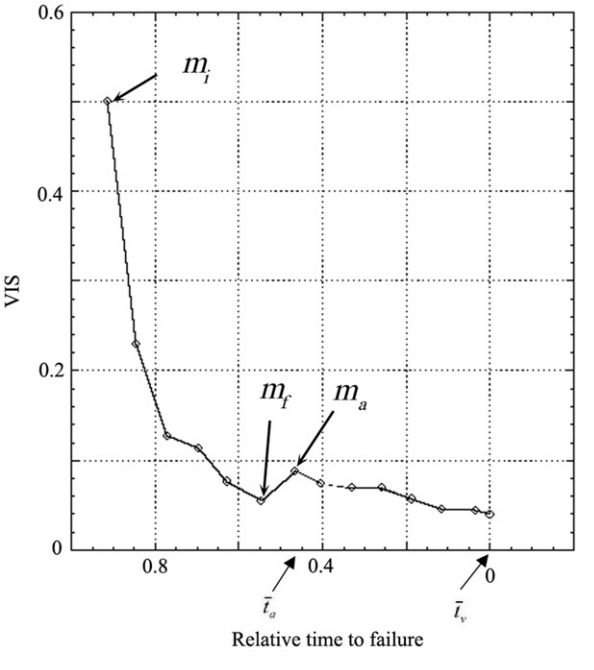

Figure 5. A schematic picture of the VIS as a function of $\bar{t}_v$: m_i is the initial slope, m_f is the slope prior to the 'bulge', and m_a is the slope at the bulge itself.

Table 1. Parameters included in the analysis for the proper 'slope at bulge' definition. Number of events for each type of failure, N, is included for the sake of comparison with the relationship given by Equation (4).

Experiment	m_i	m_f	m_a	M_{if}	L_s	M_1	N
Tension[a]	0.5	0.055	0.088	9.09	3.13	0.6	530
Compression[b]	0.32	0.051	0.08	6.27	1.49	0.57	462
Constant load compression[c]	0.152	0.056	0.093	2.71	0.98	0.66	104
Erratic load compression[c]	0.135	0.023	0.049	5.87	0.82	1.13	68
Tension[c]	0.047	0.033	0.053	1.42	0.49	0.6	31

Notes: [a]Data from recent tension experiments [19]; [b]From [13]; [c]From [20].

where $\alpha = 0.46$ (squared regression coefficient of 0.83). As we noted above, the slope m is a measure of the rate of Benioff strain release, whereas the escalation factor shows a degree of increase of the Benioff strain release relative to the Benioff strain release of the first event measured. Hence, the empirical relationship given by Equation (4) shows that when a situation becomes unstable, a specific critical correlation exists between the number of measured events, their Benioff strain release and the rate of process changes. In other words, not only a specific number of events must be registered prior to the final collapse, but also this number, the quantity related to their summarized energy (square root of energy, i.e. Benioff strain release) and the rate of the process must be interrelated. We presume that such a correlation originates from the self-correlated nature of the accelerated fracture release emerging from the combination of the loading and the stress-redistribution following the appearance of small cracks in the sample. This phenomenon is similar to the appearance of an earthquake that occurs if there exist long-range stress correlations due to a combined effect of tectonic loading and a redistribution of stress induced by previous smaller earthquakes in the region [21]. The fact that α is not a natural number may indicate a scaling, i.e. a fractal type of process.

In order to identify the 'bulge' properly, we state its attributes: (1) The VIS must have decreased sufficiently before the bulge appearance. (2) At the bulge the VIS should increase, and its relative increase should be sufficiently large.

Examination of all our experimental data measurements enables us to put forward the following quantitative relation to properly identify the bulge and the 'slope at bulge':

$$\begin{cases} m_f \le m'_a \\ M_{if} = \dfrac{m_i}{m_f} \ge 1.4 \\ M_1 = \dfrac{m_a - m_f}{m_f} \ge 0.57. \end{cases} \tag{5}$$

The first inequality means that the slope at the bulge should be higher than a minimal slope calculated by the relationship of Equation (4) at a previous point. It is the tentative 'slope at bulge' calculated on the basis of a measured m_a, the escalation factor, L_s, and the number of measured signals, N. The second inequality implies that

Table 2. Relative time left to the collapse for different experimental data sets.

Experiment	Relative time left to collapse ($\bar{t}_a$)
Tension[a]	0.46
Compression[b]	0.2
Constant load compression[c]	0.339
Erratic load compression[c]	0.148
Tension[c]	0.17

Notes: [a]Data from recent tension experiments [19]; [b]From [13]; [c]From [20].

the slope should have sufficiently decreased; the third inequality asserts that the bulge is high enough. We would like to emphasize again that the relations of Equation (5) were fulfilled by the analysis of all noted above experiments.

3.2. *'Alarm time' and 'failure time'*

The relative time of the 'slope at bulge', defined by Equation (3), is denoted as the 'alarm time' ($\bar{t}_a$), i.e. the relative time left before an oncoming failure occurs. The relative time of the failure is 0 and that of the first event is 1. Values of the alarm time for all processes appear in Table 2. As can be seen, the maximal relative time $\bar{t}_a$ is obtained for our tension experiment (0.46), whereas the minimal $\bar{t}_a$ is obtained for the erratic compression of Guarino et al. [20] (0.148).

The relative time left to failure cannot be defined before the failure itself has happened, and thus it cannot constitute a working parameter during the process. A possible criterion could be the ratio between the time left to failure (taken as the alarm time) and the time that has passed from the first event till the alarm. Such a criterion would make it possible to estimate failure time as soon as the alarm time has arrived. This ratio for the studied processes ranges between $0.148/0.852 = 17\%$ (erratic compression of Guarino et al. [20]) and $0.46/0.54 = 85\%$ (our tension experiment). It means that, once the bulge has occurred, the time left to the failure event is in the range between 15% and 85% of the time that has passed from the first event (EMR or AE) till the alarm time–time of the bulge. For example, if an hour has passed from the first detected EMR pulse till the bulge appearance, one can assess that failure could occur as soon as within 10 minutes from the bulge appearance time and that it would certainly occur during the next hour.

We have numerically studied the relationship of slope changes (between m_i and m_f, including both) and the time difference between real failure time t_c and current time t, namely $(t_c - t)$. The slopes as functions of time (from t_i to t_f) obtained from our data sets were fitted by a decaying exponential. We denoted the value, inverse to the exponential factor, as 'fall time', τ (Table 3). The failure time can then be evaluated by the following empirical relation:

$$t_c = 1.23\tau^{0.98} + t_a, \tag{6}$$

Table 3. Check for the empirical relationship of Equation (6) for all cases.

Experiment	Fall time τ(s)	$t_c - t_a$ (s)
Tension	1×10^{-13}	1.9×10^{-13}
Compression	8.7×10^{-6}	1.4×10^{-5}

with a regression coefficient of 0.9. Note that this calculation of τ is based on the regular Benioff curves and therefore is not good for predictability purposes. Moreover, the physical meaning of Equation (6) is not yet understood; that is why we would like only to note the tendency as follows:

$$t_c - t_a \sim \tau. \tag{7}$$

3.3. *Interpretation of the alarm time and the slope at the bulge*

It is conceivable that material fracturing is stimulated by an increase in stress level. This stress 'increases deterministically' by the external load. Stress release events, i.e. 'small' side fractures, however, lower the stress level in the material acting as a delaying factor to the oncoming failure. Hence, the major tentative fracture (final collapse) is somewhat shielded from the stress increase by the surrounding smaller cracks. During stress increase smaller cracks are sequentially opened and finally, when the last shielding crack has occurred, the major fracture 'bears the brunt' of the total external stress. Note that the phenomenon of crack shielding is well known in scientific literature (see, for example, [22,23]).

This stress now continues to grow with no hindrance. When finally a certain threshold (probably of a Griffith type) is overcome, major failure would result. The smaller stress release processes are registered as the accumulated Benioff strain release. The decrease of slope (Figures 4 and 5) indicates that, with time, the opposition (via a release of stress by small cracks) to the stress increase lessens gradually: this slope measures the rate of stress release which decays (almost exponentially) leading to "saturation", namely to a final inability to oppose the oncoming failure. The bulge (m_a) could be the last substantial shielding event. Following it after a specific time period ($t_c - t_a$), and depending on the rate of the whole process, the final failure ensues. We thus look for the final shielding event (m_a) after saturation has already taken place, and calculate the time period from it until the final failure.

4. Conclusion

Our analysis of the new time dependent Benioff strain release diagrams, both for different loading processes and for two different measuring techniques, i.e. EMR and AE, has shown that prior to an oncoming failure the monotonous decrease of their slope is broken by a bulge. The average relative time of the bulge buildup

is 0.33 which implies that ~33% of the overall life time of the entire failure process remains before total failure. Relative to the time from the release beginning to the bulge (note that the proceeding should not be retrospective), it means, on the average, that about half of this time is left till the failure. This paper deals with a few experimental data sets, because its aim is to introduce a new method for failure forecasting. More statistical data has of course to be processed using this method, to improve the criteria suggested.

References

[1] V.G. Kossobokov, V.I. Keilis-Borok and B. Cheng, Phys. Rev. E 61 (2000) p.3529.
[2] D.D. Bowman, G. Ouillon, C.G. Sammis, D. Sornett and A. Sornette, J. Geophys. Res. 103 (1998) p.24.
[3] D.D. Bowman, G. Ouillon, C.G. Sammis, D. Sornett and A. Sornette, J. Geophys. Res. 103 (1998) p.359.
[4] M. Wyss, Tectonophysics 338 (2001) p.217.
[5] Y. Ben-Zion and V. Lyakhovsky, Pure Appl. Geophys. 159 (2002) p.2385.
[6] S.C. Jaume, D. Weatherley and P. Mora, Pure Appl. Geophys. 157 (2000) p.2209.
[7] C.G. Bufe and D.J. Varnes, J. Geophys. Res. 98 (1993) p.9871.
[8] H.H. Zhang, X.C. Yin, N.G. Liang, H.Z. Yu, S.Y. Li, Y. Wang, C. Yin, V. Kuksenko, N. Tomiline and S. Elizarov, Pure Appl. Geophys. 163 (2006) p.2389.
[9] Y. Kawada and H. Nagahama, Tectonophysics 424 (2006) p.157.
[10] Y. Kawada, H. Nagahama and N. Nakamura, Nat. Hazards Earth Syst. Sci. 7 (2007) p.599.
[11] A. Rabinovitch, V. Frid and D. Bahat, Phys. Rev. E 65 (2002) p.011401.
[12] C. Mavromatou, G.S. Tombras and D. Ninos, J. Appl. Phys. 103 (2008) p.083518.
[13] A. Rabinovitch, V. Frid and D. Bahat, Tectonophysics 431 (2007) p.15.
[14] F. Vallianatos and D. Triantis, Physica A 387 (2008) p.4940.
[15] A. Tsutsumi and N. Shirai, Tectonophysics 450 (2008) p.79.
[16] J. Mallik, G. Mathew and T. Angerer, J. Geodyn. 45 (2008) p.234.
[17] K. Fukui, S. Okubo and T. Terashima, Rock Mech. Rock Eng. 38 (2005) p.411.
[18] I. Stavrakas, D. Triantis and Z. Agioutantis, Nat. Hazards Earth Syst. Sci. 4 (2004) p.563.
[19] V. Frid, A. Rabinovitch and D. Bahat, Phys. Lett. A 356 (2006) p.160.
[20] A. Guarino, S. Ciliberto, A. Garcimartin, M. Zei and R. Scorretti, Eur. Phys. J. B 26 (2002) p.141.
[21] S.C. Jaume, D. Weatherley and P. Mora, Pure Appl. Geophys. 157 (2000) p.2209.
[22] J.W. Hutchinson, Acta Metall. 35 (1987) p.1605.
[23] S.B. Biner, Eng. Fract. Mech. 51 (1995) p.555.